JUSTC

Article

http://justc.ustc.edu.cn

Received: April 02, 2024; Accepted: July 24, 2024

Effects of the wavy leading-edge wavelength on the reduction in the noise of the rod–airfoil configuration

Fuyang Yu, Zhenhua Wan ✉, Yasen Hu, and Dejun Sun

Department of Modern Mechanics, University of Science and Technology of China, Hefei 230027, China

✉Correspondence: Zhenhua Wan, E-mail: wanzh@ustc.edu.cn

Graphical abstract

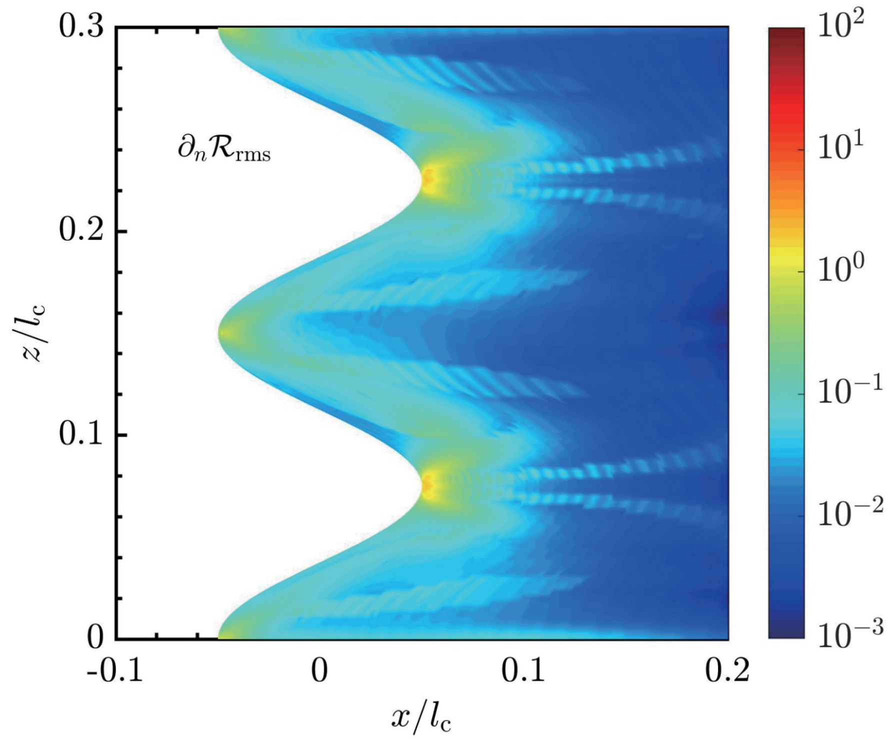

The noise production induced by WLEs is diagnosed via multiprocess acoustic theory.

Public summary

■ The effect of a wavy leading-edge wavelength on rod–airfoil noise reduction is examined.

■ Noise reduction mechanisms are revealed quantitatively via the theory of multiprocess aeroacoustics.

■ Reducing the wavelength is favorable for enhancing the source cutoff effect and destructive source relationship.

Citation: Yu F Y, Wan Z H, Hu Y S, et al. Effects of the wavy leading-edge wavelength on the reduction in the noise of the rod–airfoil configuration. *JUSTC*, **2025**, 55(2): 0202. CSTR: 32290.14.JUSTC-2024-0053. DOI: 10.52396/JUSTC-2024-0053

JUSTC

Article

http://justc.ustc.edu.cn

Received: April 02, 2024; Accepted: July 24, 2024

Effects of the wavy leading-edge wavelength on the reduction in the noise of the rod–airfoil configuration

Fuyang Yu, Zhenhua Wan ✉, Yasen Hu, and Dejun Sun

Department of Modern Mechanics, University of Science and Technology of China, Hefei 230027, China

✉Correspondence: Zhenhua Wan, E-mail: wanzh@ustc.edu.cn

Cite This: *JUSTC*, **2025**, 55(2): 0202 (7pp)   Read Online

Abstract: Rod–airfoil interaction noise becomes a major issue in some aeronautical applications. The design of four wavy leading edges (WLEs) with varying wavelengths, bioinspired by the tubercles on humpback whales' flippers, aims to mitigate far-field noise. Among these cases, a reduction in the wavelength is found to be advantageous for noise suppression, with the smallest wavelength case achieving a maximum noise reduction of 1.9 dB. Furthermore, the noise radiation induced by WLEs is suppressed mainly at medium frequencies. The theory of multiprocess aeroacoustics is applied to reveal their underlying mechanisms. The dominant factor is the source cutoff effect, which significantly decreases the source strength on hills. Additionally, spanwise decoherence with phase interference serves as another crucial mechanism, particularly for reducing mid-frequency noise.

Keywords: rod–airfoil; wavy leading edge; wavelength; multiprocess acoustic theory

CLC number: O422.8; O35   **Document code:** A

1 Introduction

In recent decades, airfoil–turbulence interaction (ATI) noise has become a popular research topic. Among them, the study of rod–airfoil configurations has attracted considerable attention since it is a simplified model of rotor-stator interactions in turbofans[1–6]. Extensive studies have demonstrated that the rod–airfoil flow exhibits two typical modes: a wake pattern with a large interaction gap and a vortex suppression pattern with a small interaction gap[7,8]. In the wake mode, the vortex impingement on the leading edge of the airfoil is the primary source of noise. In recent years, several approaches have been used to reduce ATI noise, such as natural blowing[4,9], porous surfaces[4,10–12], and geometric modifications[13–15].

Motivated by the silent flight of owls and the exceptional lift-enhancing and drag-reducing performance exhibited by humpback whale flippers, the utilization of a wavy leading edge (WLE) has been acknowledged as a promising approach for mitigating ATI noise[16,17]. The effect of the WLE amplitude on noise reduction in isotropic or grid-generated turbulence has been extensively discussed in previous studies[18–20], and a general finding is that increasing the amplitude tends to achieve better noise reduction. The noise reduction capability is also associated with the wavelength of the incident gust[18]. To date, the effect of the WLE wavelength on noise reduction has remained controversial. Chong et al.[21] reported that a small serrated wavelength is beneficial for decreasing noise. In turn, Narayanan et al.[19] reported that better noise reduction was obtained with wider series. Chaitanya et al.[20] revealed that the optimal serrated wavelength corresponds to a quarter of the length scale of the turbulent integral. In the experiments of Chen et al.[14], no optimal serrated wavelength was found to be present. The lack of studies on relatively realistic turbulence, such as the rod–airfoil configuration, necessitates a numerical investigation to evaluate the influence of the WLE wavelength on the noise attenuation capability.

The noise reduction induced by WLE may involve more than one mechanism. Lau et al.[18] suggested that the incoherent response to the turbulence induced by WLE contributes to noise reduction. Chaitanya et al.[20] associated the best wavelength with incoherent adjacent sources. Narayanan et al.[19] highlighted that spanwise decoherence and phase variation are the key factors. Similar mechanisms were found in numerical studies by Chen et al.[15] and several analytical models (Ayton et al.[22,23] and Lyu et al.[24]). Kim et al.[25] suggested that the source cutoff effect also plays an essential role. Recently, with the development of numerical simulations, the diagnosis of near-field sources on the basis of multiprocess acoustic theory has become possible[26,27]. In the present work, we provide a physical explanation of noise reduction with the aid of this theory.

The remainder of the paper is organized as follows. Section 2 presents the computational overview and theory of multiprocess aeroacoustics. Section 3 presents the acoustic performance of WLEs with various wavelengths and discusses the noise mitigation mechanisms. Finally, the key findings are presented in Section 4.

2 Computational approaches and multiprocess acoustic theory

2.1 Computational overview

The flow conditions of the simulation are similar to those of

CSTR: 32290.14.JUSTC-2024-0053
DOI: 10.52396/JUSTC-2024-0053
JUSTC, **2025**, 55(2): 0202

the experiment performed by Jacob et al[3]. The schematic diagram is shown in Fig. 1. A NACA-0012 airfoil (chord length $l_c = 0.1$ m) is placed 0.1 m downstream of a cylindrical rod (diameter $d = 0.01$ m). The spanwise length l_z in the numerical simulation is $3d$. This rod–airfoil configuration is put in a uniform inflow ($Ma = 0.21$, $T_0 = 293$ K, $\rho_0 = 1.2$ kg/m^3). The Reynolds number based on the airfoil chord length is 4.8×10^5.

The turbulent flow is solved through the compressible large-eddy simulation (LES) using an unstructured grid with the finite volume method. To avoid spurious reflections, the sponge zone technique is introduced along the Riemann far field. In addition, an adiabatic no-slip wall is implemented on the rod and airfoil surfaces, together with a slip wall imposed in the spanwise direction. The convection terms are discretized by the Roe scheme. The lower-upper symmetric Gauss-Seidel (LU-SGS) method is applied for time marching. The subgrid-scale eddy viscosity is obtained through the σ model[28]. In the present study, the flow simulation is performed by the open-source solver PHengLEI[29]. Details of the numerical methods are given in Ref. [29].

The Ffowcs-Williams Hawkings (FW-H) analogy is applied to calculate the noise in the far field with the fluctuation quantities on the integral surface obtained via LES[30]. The FW-H permeable surface is represented by the red line in Fig. 1. No volume integration is performed because the quadrupole source can be overlooked at low speeds. Noise signals are collected at intervals of 6.59×10^{-6} s. With Kato's method[31], we correct the sound pressure level (SPL) for the spanwise difference between the simulation and the experiment.

A series of sinusoidal leading shapes with various wavelengths W is designed to mitigate the rod–airfoil noise. At present, the four wavy cases, W150, W100, W075, and W050, are named for their wavelengths. For example, the case W075 has a wavelength $W = 0.075l_c$. All wavy curves have the same amplitude, that is, $A = 0.1l_c$. The grids used for all the cases have a similar topology, with only a slightly different number of cells. The computational mesh is shown in Fig. 2. We use structured meshes around the cylinder and airfoil. In the wake region of the airfoil, the structured mesh is also applied. The expansion ratio of the boundary layer mesh

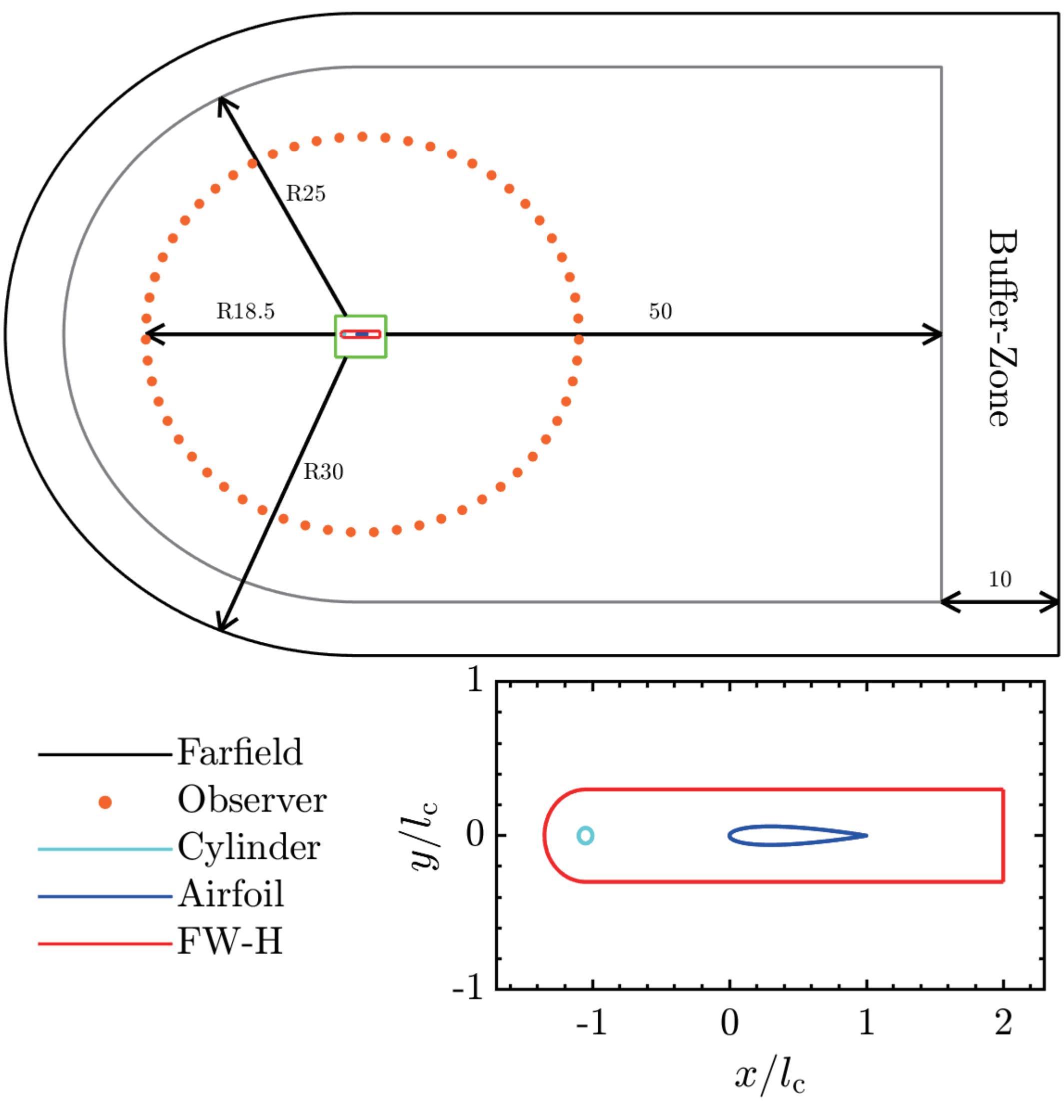

Fig. 1. A schematic diagram of the rod–airfoil. The buffer region, FW-H permeable surface, and far-field observers are given.

CSTR: 32290.14.JUSTC-2024-0053
DOI: 10.52396/JUSTC-2024-0053
JUSTC, **2025**, 55(2): 0202

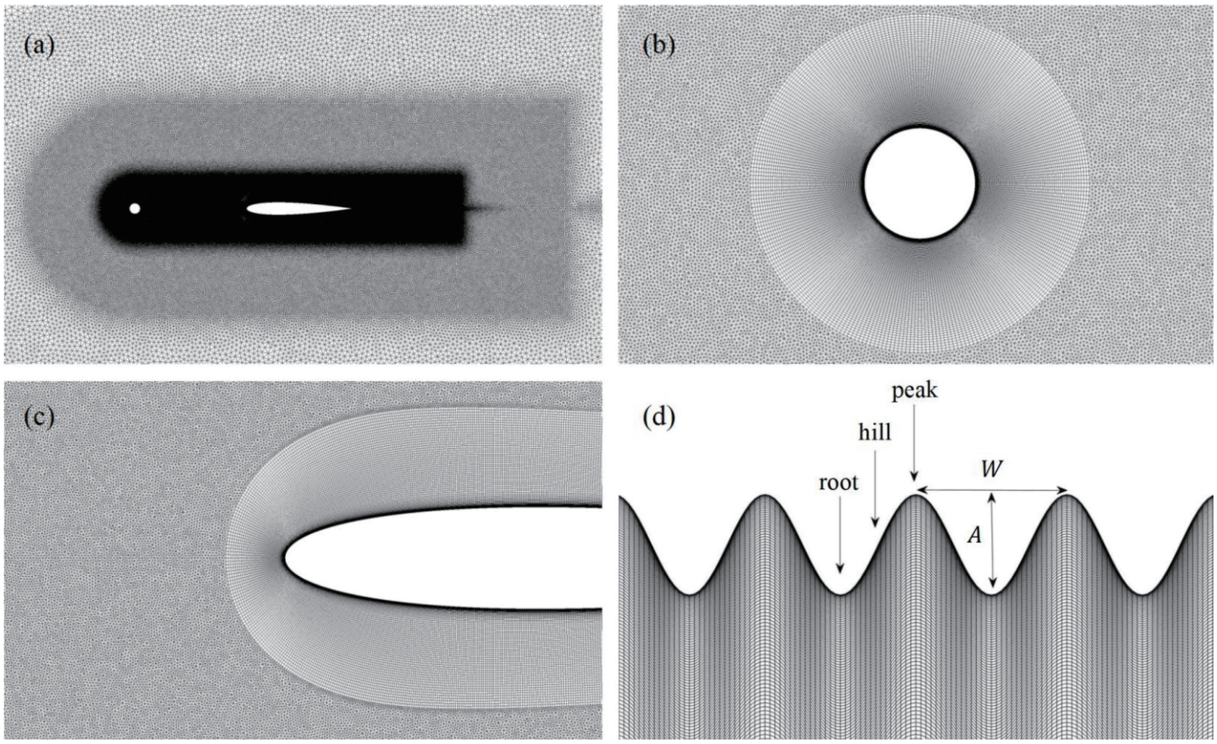

Fig. 2. Sketch of the mesh. (a) Overall view. (b) Enlarged view in the vicinity of the rod. (c) Enlarged view in the vicinity of the airfoil leading edge for the SLE case. (d) Local mesh topology of the wavy leading edge for case W075.

is 1.05, and the grid density of the first layer is set to satisfy $\Delta y^+ < 1$. Unstructured cells are filled elsewhere. The straight case SLE contains approximately 73 million cells. At least 30 grid points per serration period in the spanwise direction are arranged to ensure sufficient resolution. The surface mesh of W075 is illustrated in Fig. 2d.

The present SPL spectra are compared with the previous simulation and experimental results at a far-field point ($x/l_c = 6.8$, $y/l_c = 17.4$, $z/l_c = 0.15$) in Fig. 3 to validate the LES results. Our findings are in good agreement with those of prior investigations[3,32].

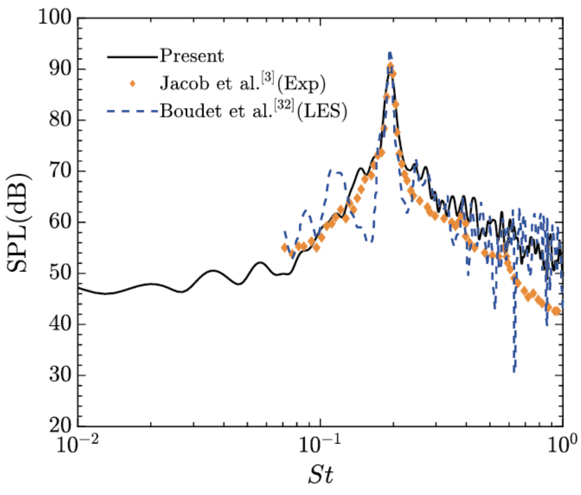

Fig. 3. Comparisons of sound pressure level (SPL) at the observer of ($x/l_c = 6.8$, $y/l_c = 17.4$, $z/l_c = 0.15$).

2.2 Multiprocess acoustic theory

There is no doubt that FW-H theory has succeeded in predicting far-field noise. However, the sources used in the analogy are not equal to physical noise sources and cannot effectively reveal the connection between acoustic sources and flow structures. The theory of multiprocess aeroacoustics recently proposed by Mao et al.[26,33] is expected to overcome this challenge to some degree. Here, $\mathcal{R} = \ln(\rho/\rho_0)$ is treated as the dimensionless acoustic variable, and the noise source is defined by the objective causality intrinsic to the dynamic equations associated with longitudinal processes. The acoustic equation is expressed as:

$$D^2\mathcal{R} - \nabla\cdot(c^2\nabla\mathcal{R}) - (D\mathcal{R})^2 - \nu_\theta\nabla^2 D\mathcal{R} = \nabla\cdot(c^2\nabla s^*) - \beta, \quad (1)$$

where D is the operator of the material derivative, ν_θ denotes the viscosity of the longitudinal kinematics, and c is the sound speed. Here, $\beta = (\vartheta\boldsymbol{I} - \nabla\boldsymbol{u}^{\mathrm{T}}) : \nabla\boldsymbol{u}$ denotes the kinematic source of the acoustic mode, where $\boldsymbol{I}$ represents a second-order unit tensor and ϑ represents the dilatation. β is considered as a pseudo 'inviscid work rate' made by the nonlinear inertial force on the boundary of the unit mass control volume. The entropy part $\nabla\cdot(c^2\nabla s^*)$ is overlooked owing to the low Mach condition. In contrast to the FW-H theory, the current source terms are more physical, which excludes the hydrodynamic components and allows a direct description of the shear and thermodynamic processes contributing to sound production.

For the rod–airfoil interactions, the sound generated by the wall must be considered[34]. Therefore, the momentum equation is applied to the boundary. The momentum equation in the form of dimensionless thermodynamic variables is

CSTR: 32290.14.JUSTC-2024-0053
DOI: 10.52396/JUSTC-2024-0053
JUSTC, **2025**, 55(2): 0202

expressed as follows:

$$-\nabla\mathcal{P}=\frac{1}{c^2}(\boldsymbol{a}-\boldsymbol{\eta})=-\nabla\left(-\frac{1}{\gamma-1}s^*+\mathcal{T}\right), \tag{2}$$

where $\boldsymbol{a}\equiv D\boldsymbol{u}$ is the acceleration, $\boldsymbol{\eta}\equiv\nu_\theta\nabla\vartheta-\nu\nabla\times\boldsymbol{\omega}$ denotes the viscous force of a unit mass, and ν denotes the vorticity and shear kinematic viscosity, respectively. If the acceleration of the wall $\boldsymbol{a}=\boldsymbol{a}_{\rm w}(\boldsymbol{x},t)$ is given, the flux of pressure on the boundary is:

$$\partial_n\mathcal{P}=\partial_n\left(-\frac{s^*}{\gamma-1}+\mathcal{T}\right)=\frac{1}{c^2}\boldsymbol{n}\cdot(\boldsymbol{\eta}_{\rm w}-\boldsymbol{a}_{\rm w}). \tag{3}$$

Neglecting the entropy change, the state equation for a perfect gas is as follows:

$$s^*=-\mathcal{R}+\mathcal{P}\approx 0. \tag{4}$$

In this study, all the objects are stationary; thus, the sound mode equation at the boundary is simplified in the following form:

$$\partial_n\mathcal{R}\approx\frac{1}{c^2}\boldsymbol{n}\cdot[\nu_\theta\partial_n\vartheta-\nu(\boldsymbol{n}\times\nabla)\cdot\omega]. \tag{5}$$

Currently, the acoustic sources in the field and the sound generation on the wall are diagnosed by β and $\partial_n\mathcal{R}$, respectively.

3 Results and discussion

3.1 Variations in noise reduction with wavelength

A parametric investigation is conducted to determine the relationship between noise reduction and the WLE wavelength. The overall sound pressure levels (OASPLs) of various cases are given in Fig. 4. The definition of OASPL is as follows:

$$\mathrm{OASPL}=20\log_{10}(p'_{\rm rms}/p_{\rm ref}), \tag{6}$$

where the reference pressure $p_{\rm ref}$ is 2×10^{-5} Pa. Some degree of noise reduction is achieved for all the WLEs, with no distinct change in the propagation direction. Overall, within the current parameter range, reducing the wavelength helps reduce noise. The W050 with the minimum wavelength obtained a noise reduction of up to 1.9 dB in the main propagation direction (approximately 70°). In other directions, e.g., 120°, the maximum noise reduction is approximately 3.2 dB.

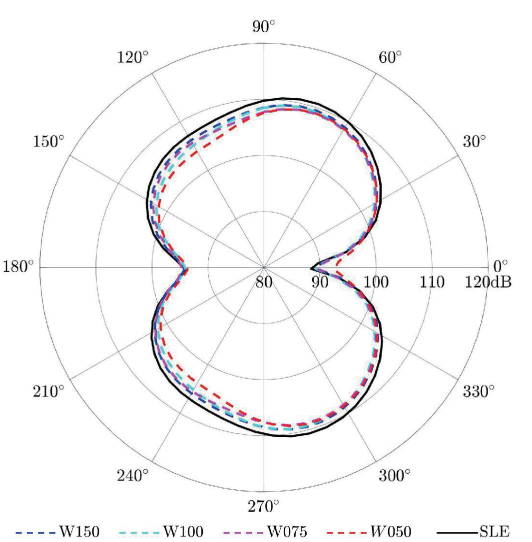

Fig. 4. The overall sound pressure levels (OASPL) ($R=1.85$ m) for all cases.

Furthermore, we evaluate the noise suppression performance in different frequency ranges. The mean overall sound power reduction level (ΔOAPWL) from 45° to 135° is calculated as follows:

$$W(f)=\frac{l_zR}{\rho_0c}\left(\sum_{i=1}^{N-1}\left(\frac{S_{pp}(f,\theta_{i+1})+S_{pp}(f,\theta_i)}{2}\right)\Delta\theta\right),\ 45^\circ<\theta<135^\circ, \tag{7}$$

$$\mathrm{PWL}(f)=10\log_{10}(W(f)/W_{\rm ref}), \tag{8}$$

$$\mathrm{OAPWL}=10\log_{10}\left(\frac{1}{St_{\rm up}-St_{\rm down}}\int_{St_{\rm down}}^{St_{\rm up}}(W(f)/W_{\rm ref})\mathrm{d}St\right), \tag{9}$$

$$\Delta\mathrm{OAPWL}=\mathrm{OAPWL}_{\rm SLE}-\mathrm{OAPWL}_{\rm WLE}, \tag{10}$$

where $R=1.85$ m, $\Delta\theta=6^\circ\times\pi/180$, and $W_{\rm ref}=10^{-12}$ W. Four different ranges are evaluated: the low-frequency range $St=[0,0.1]$, the medium-frequency range $St=[0.1,0.3]$ (the vortex tonal noise is included), $St=[0.3,1]$ and the high-frequency range $St=[1,10]$. As shown in Fig. 5, noise reduction mainly occurs in the medium frequency band. Among them, the W050 achieves a 3.9 dB noise reduction at $St=[0.3,1]$. Additionally, an inversely proportional relationship between the ΔOAPWL and WLE wavelengths at $St=[0.1,1]$ means that decreasing the wavelength is beneficial for noise mitigation. In the low-frequency band, the moderate-wavelength case W100 achieves the greatest noise reduction, whereas the small-wavelength case W050 shows a slight increase in noise. In the high-frequency band, noise reduction is less effective, except in the W050 case. It should be reported that high-frequency noise is associated with airfoil

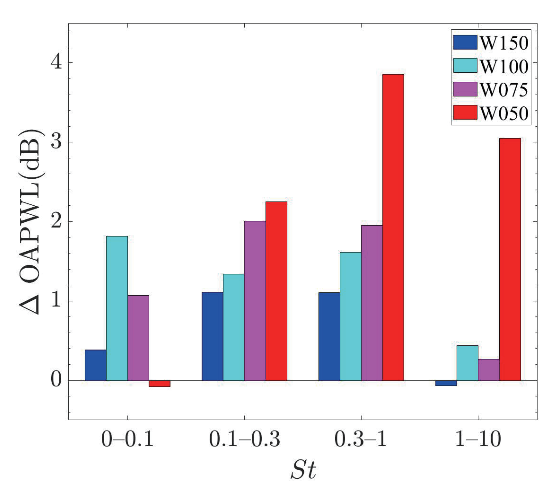

Fig. 5. The mean overall sound power reduced level (ΔOAPWL) in the different frequency bands.

CSTR: 32290.14.JUSTC-2024-0053
DOI: 10.52396/JUSTC-2024-0053
JUSTC, **2025**, 55(2): 0202

self-noise and is not the main focus of the present study.

3.2 Noise reduction mechanisms

In the previous section, we were unable to observe the optimal wavelength mentioned in isotropic turbulence by Chaitanya et al[20]. In rod–airfoil interactions, the degree of noise reduction is negatively correlated with the WLE wavelength and comes mainly from the medium frequency band. To elucidate the noise reduction mechanisms, we first investigate the change in the noise source due to WLE.

To quantify the intensity of the noise source, we resort to the multiprocess aeroacoustic theory that was mentioned before. In Fig. 6a–c, $\partial_n\mathcal{R}$ is plotted to represent the noise generated by the wall. In Fig. 6d–f, β is utilized to denote the noise sources in the near-wall space. Given the similar distributions of $\partial_n\mathcal{R}$ and β in this case, we collectively refer to them as sound sources in the following analysis. In Fig. 6, the leading edge of the airfoil is the main sound source region. The sound source characteristics of WLE and SLE are significantly different. The dominant sound sources of WLEs are confined to the peaks and roots, while the noise intensity of the hills significantly decreases. This finding is consistent with the source cutoff effect proposed in isotropic turbulence by Kim et al[25]. The definitions of peaks, roots, and hills are given in Fig. 2. Comparisons of the W150 and W050 sources reveal that the cutoff effect is more powerful in the small wavelength case. In brief, a notable decrease in the intensity of hill sources is one of the main noise reduction mechanisms.

Apart from the intensity of the sources, the interference effect between the sources also plays a role in far-field noise. Fig. 7 compares the spanwise averaged coherence spectra of various cases. The definition of $C_{pp}(z_2:z_1,f)$ is as follows:

$$C_{pp}(z_2:z_1,f)=\frac{\left|\langle S_{pp}(z_2:z_1,f)\rangle\right|^2}{\langle|S_{pp}(z_2,f)|^2\rangle\langle|S_{pp}(z_1,f)|^2\rangle}, \tag{11}$$

$$C_{pp}(f)=\frac{1}{l_z}\int_0^{l_z}C_{pp}(z_2:z_1,f)\,\mathrm{d}z, \tag{12}$$

where

$$S_{pp}(z,f)=2\hat{p}^*(z,f)\hat{p}(z,f), \tag{13}$$

$$S_{pp}(z_2:z_1,f)=2\hat{p}^*(z_1,f)\,\hat{p}(z_2,f), \tag{14}$$

where, "^" represents the Fourier transform and "*" denotes the complex conjugate. Compared with SLE, the spanwise coherence of WLEs decreases at almost all frequencies. The impact of WLE on the mid-frequency band is prominent, especially the significant drop of the coherence peaks at the vortex tonal frequency ($St=0.1938$) and the frequency of drag oscillation ($St=0.3876$). Although the variations are not monotonic, small wavelength cases tend to attain low coherence levels.

The phase variation on the leading edge is shown in Fig. 8. The definition of phase ϕ is as follows:

$$\phi(z_2:z_1,f)=\mathrm{Im}\left[\ln(S_{pp}(z_2:z_1,f))\right], \tag{15}$$

where Im denotes the imaginary part. $\cos(\phi)=1$ denotes in-phase radiation, and $\cos(\phi)=-1$ denotes out-of-phase radiation. It is obvious that the additional phase changes induced by WLE are concentrated in the medium frequency band, as shown in the green box. The smaller wavelength case, e.g., W050, has a deeper degree of phase interference. Notably, achieving perfect phase interference in rod–airfoil

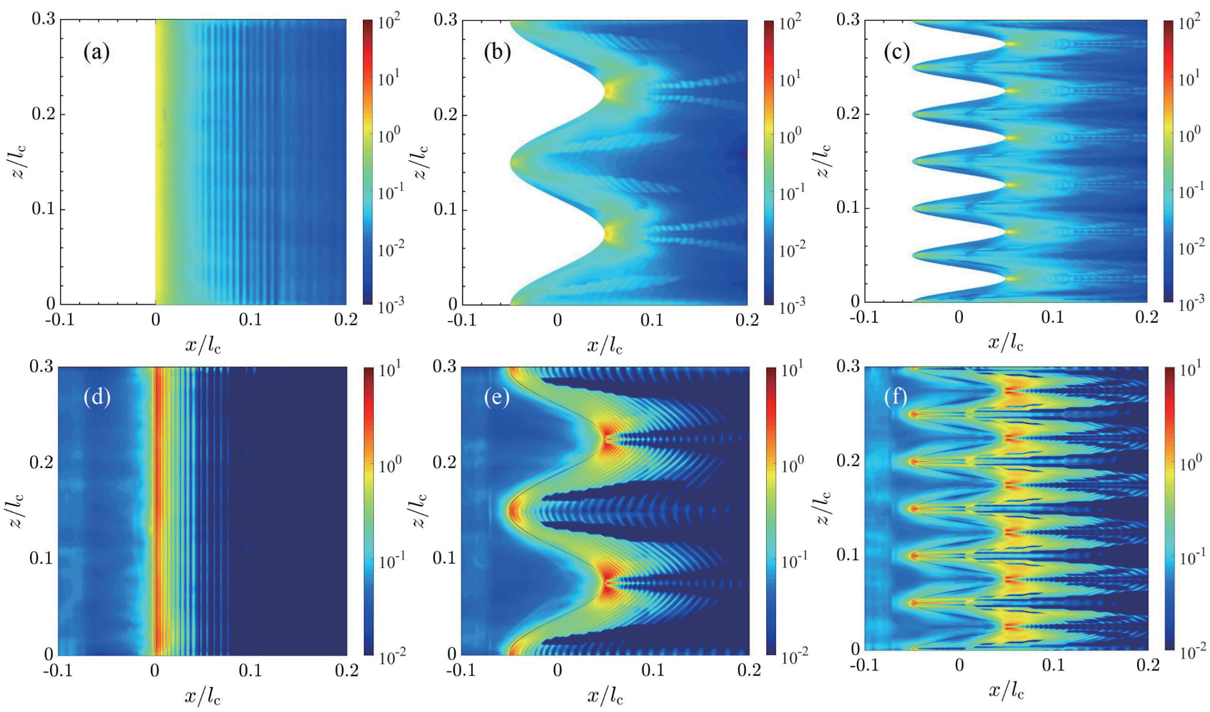

Fig. 6. The sound generated by the wall and the acoustic sources in the field are diagnosed by $\partial_n\mathcal{R}_{\rm rms}$ and $\sqrt{\langle\beta^2\rangle}$, respectively. Each value is normalized via the mean of the SLE. $\partial_n\mathcal{R}_{\rm rms}$ of (a) the SLE case, (b) the W150 case, and (c) the W050 case. $\sqrt{\langle\beta^2\rangle}$ of (d) the SLE case, (e) the W150 case, and (f) the W050 case.

CSTR: 32290.14.JUSTC-2024-0053
DOI: 10.52396/JUSTC-2024-0053
JUSTC, **2025**, 55(2): 0202

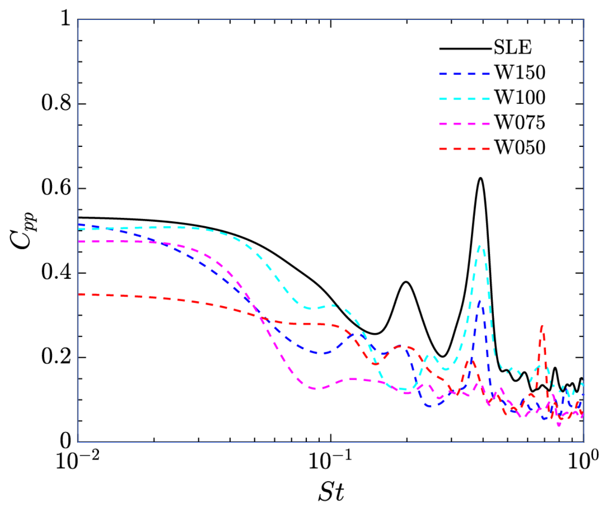

Fig. 7. Spanwise averaged profiles of the coherence spectra. The center point of the leading edge is chosen as the reference point.

interactions is much more challenging, which may explain the difficulty in theoretically finding the optimal wavelength. As shown in the yellow box, for low-frequency components, sources tend to radiate in phase. Moreover, small wavelengths introduce a slight low-frequency out-of-phase. In conclusion, both the spanwise decoherence and variation in the phase play crucial roles in medium-frequency noise reduction.

4 Conclusions

Large-eddy simulations are employed to investigate the flow structures and sound radiation in the rod–airfoil model. The leading edges of four wavy airfoils with various wavelengths are designed to reduce the far-field noise. The noise reduction performance is negatively correlated with the wavelength. The W050 with the minimum wavelength achieves an approximately 1.9 dB noise reduction in the dominant propagation direction. The wavy leading edge is most effective at moderate frequencies $St = [0.1, 1]$, reducing noise up to 3.9 dB.

The theory of multiprocess aeroacoustics is applied to the diagnosis of noise production by the wall and near-wall space, respectively. The source cutoff effect is considered a crucial mechanism. The dominant sources are confined to the peak and root regions, and the noise intensity at hills is distinctly reduced. The spanwise decoherence with phase interference is another noise reduction mechanism, especially in mid-frequency noise mitigation ($St = [0.1, 1]$). Smaller wavelengths contribute to a greater source cutoff and phase interference.

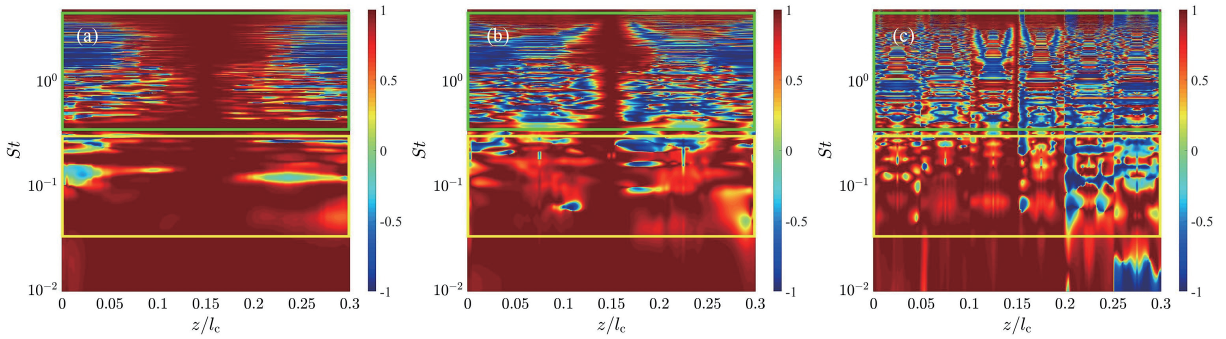

Fig. 8. $\cos(\phi)$ is used to show the phase variation along the airfoil leading edge. (a) SLE. (b) W150. (c) W050. The midpoint of the airfoil leading edge is chosen as the reference point.

Acknowledgements

This work was supported by the National Natural Science Foundation of China (12322210, 12172351, 92252202, and 12388101) and the Fundamental Research Funds for the Central Universities.

Conflict of interest

The authors declare that they have no conflict of interest.

Biographies

Fuyang Yu is currently a Ph.D. candidate at the Department of Modern Mechanics, University of Science and Technology of China (USTC). He received his bachelor's degree from USTC in 2021. His research interests mainly focus on the noise reduction design, mechanisms, and optimization control of airfoils and blades.

Zhenhua Wan is currently a Professor at the Department of Modern Mechanics, University of Science and Technology of China (USTC). He received his bachelor's degree from Northwestern Polytechnical University in 2008 and his Ph.D. degree from USTC in 2013. His research interests mainly focus on the efficient simulation and control of compressible turbulent flow and aerodynamic noise.

References

[1] Tyler J M, Sofrin T. Axial flow compressor noise studies. *SAE Transactions*, **1962**, *70*: 309.

[2] Casalino D, Diozzi F, Sannino R, et al. Aircraft noise reduction technologies: A bibliographic review. *Aerospace Science and Technology*, **2008**, *12*: 1–17.

[3] Jacob M C, Boudet J, Casalino D, et al. A rod-airfoil experiment as a benchmark for broadband noise modeling. *Theoretical and Computational Fluid Dynamics*, **2005**, *19*: 171–196.

[4] Li Y, Wang X N, Chen Z W, et al. Experimental study of vortex–structure interaction noise radiated from rod–airfoil configurations. *Journal of Fluids and Structures*, **2014**, *51*: 313–325.

[5] Sharma S, Geyer T F, Giesler J. Effect of geometric parameters on the noise generated by rod-airfoil configuration. *Applied Acoustics*, **2021**, *177*: 107908.

[6] Li Y, Niu X. Rod–airfoil interaction noise at different rod cross

sections and airfoil angles. *AIAA Journal*, **2022**, *60*: 3635–3650.

[7] Jiang Y, Mao M L, Deng X G, et al. Numerical investigation on body-wake flow interaction over rod–airfoil configuration. *Journal of Fluid Mechanics*, **2015**, *779*: 1–35.

[8] Eltaweel A, Wang M. Numerical simulation of broadband noise from airfoil-wake interaction. In: 17th AIAA/CEAS Aeroacoustics Conference (32nd AIAA Aeroacoustics Conference). Oregon, Portland: AIAA, **2012**: 2802.

[9] Li Y, Chen Z, Wang X. Flow/noise control of a rod–airfoil configuration using "natural rod-base blowing": Numerical experiments. *European Journal of Mechanics - B/Fluids*, **2020**, *83*: 99–113.

[10] Zamponi R, Satcunanathan S, Moreau S, et al. On the role of turbulence distortion on leading-edge noise reduction by means of porosity. *Journal of Sound and Vibration*, **2020**, *485*: 115561.

[11] Teruna C, Avallone F, Casalino D, et al. Numerical investigation of leading edge noise reduction on a rod-airfoil configuration using porous materials and serrations. *Journal of Sound and Vibration*, **2021**, *494*: 115880.

[12] Wang Y, Tong F, Chen Z, et al. Rod–airfoil interaction noise reduction using gradient distributed porous leading edges. *Applied Sciences*, **2022**, *12* (10): 4941.

[13] Agrawal B R, Sharma A. Numerical analysis of aerodynamic noise mitigation *via* leading edge serrations for a rod–airfoil configuration. *International Journal of Aeroacoustics*, **2016**, *15*: 734–756.

[14] Chen W, Qiao W, Tong F, et al. Experimental investigation of wavy leading edges on rod-aerofoil interaction noise. *Journal of Sound Vibration*, **2018**, *422*: 409–431.

[15] Chen W, Qiao W, Tong F, et al. Numerical investigation of wavy leading edges on rod–airfoil interaction noise. *AIAA Journal*, **2018**, *56*: 2553–2567.

[16] Graham R R. The silent flight of owls. *Journal of the Royal Aeronautical Society*, **1934**, *38* (286): 837–843.

[17] Fish F E, Weber P W, Murray M M, et al. The tubercles on humpback whales' flippers: Application of bio-inspired technology. *Integrative and Comparative Biology*, **2011**, *51*: 203–213.

[18] Lau A S H, Haeri S, Kim J W. The effect of wavy leading edges on aerofoil–gust interaction noise. *Journal of Sound and Vibration*, **2013**, *332*: 6234–6253.

[19] Narayanan S, Chaitanya P, Haeri S, et al. Airfoil noise reductions through leading edge serrations. *Physics of Fluids*, **2015**, *27*: 025109.

[20] Chaitanya P, Joseph P, Narayanan S, et al. Performance and mechanism of sinusoidal leading edge serrations for the reduction of turbulence–aerofoil interaction noise. *Journal of Fluid Mechanics*, **2017**, *818*: 435–464.

[21] Chong T P, Vathylakis A, McEwen A, et al. Aeroacoustic and aerodynamic performances of an aerofoil subjected to sinusoidal leading edges. In: 21st AIAA/CEAS Aeroacoustics Conference. Dallas, TX, USA: AIAA, **2015**: 2015–2200.

[22] Ayton L J, Kim J W. An analytic solution for the noise generated by gust–aerofoil interaction for plates with serrated leading edges. *Journal of Fluid Mechanics*, **2018**, *853*: 515–536.

[23] Ayton L J, Chaitanya P. An analytical and experimental investigation of aerofoil–turbulence interaction noise for plates with spanwise-varying leading edges. *Journal of Fluid Mechanics*, **2019**, *865*: 137–168.

[24] Lyu B, Azarpeyvand M. On the noise prediction for serrated leading edges. *Journal of Fluid Mechanics*, **2017**, *826*: 205–234.

[25] Kim J W, Haeri S, Joseph P F. On the reduction of aerofoil–turbulence interaction noise associated with wavy leading edges. *Journal of Fluid Mechanics*, **2016**, *792*: 526–552.

[26] Mao F, Kang L L, Wu J Z, et al. A study of longitudinal processes and interactions in compressible viscous flows. *Journal of Fluid Mechanics*, **2020**, *893*: A23.

[27] Hu Y S, Wan Z H, Ye C C, et al. Noise reduction mechanisms for insert-type serrations of the NACA-0012 airfoil. *Journal of Fluid Mechanics*, **2022**, *941*: A57.

[28] Nicoud F, Toda H B, Cabrit O, et al. Using singular values to build a subgrid-scale model for large eddy simulations. *Physics of Fluids*, **2011**, *23*: 085106.

[29] Zhao Z, He L, He X Y. Design of general CFD software PHengLEI. *Computer Engineering and Science*, **2020**, *42* (2): 210–219. (in Chinese)

[30] Casalino D. An advanced time approach for acoustic analogy predictions. *Journal of Sound and Vibration*, **2003**, *261*: 583–612.

[31] Kato C, Iida A, Takano Y, et al. Numerical prediction of aerodynamic noise radiated from low Mach number turbulent wake. In: 31st Aerospace Sciences Meeting. Reston, VA, USA: AIAA, **1993**: 145.

[32] Boudet J, Casalino D, Jacob M, et al. Prediction of broadband noise: Airfoil in the wake of a rod. In: 42nd AIAA Aerospace Sciences Meeting and Exhibit. Reston, VA, USA: AIAA, **2004**: 852.

[33] Mao F, Liu L, Kang L, et al. A unified theory for gas dynamics and aeroacoustics in viscous compressible flows. Part II. Sources on solid boundary. *Acta Mechanica Sinica*, **2022**, *38*: 321583.

[34] Yu F Y, Wan Z H, Hu Y S, et al. Analysis of wavy leading-edge noise reduction and source mechanism in rod-airfoil interactions. *Physics of Fluids*, **2024**, *36*: 045122.

CSTR: 32290.14.JUSTC-2024-0053
DOI: 10.52396/JUSTC-2024-0053
JUSTC, **2025**, 55(2): 0202